OPEN

Objective CT-Based Quantification of Lung Sequelae in Treated Patients With Paracoccidioidomycosis

Matheus Alvarez, MSc, Diana R. Pina, PhD, Marcela de Oliveira, MSc, Sérgio M. Ribeiro, MD, Rinaldo P. Mendes, PhD, Sérgio B. Duarte, PhD, and José R.A. Miranda, PhD

Abstract: This study presents methodology for objectively quantifying the pulmonary region affected by emphysemic and fibrotic sequelae in treated patients with paracoccidioidomycosis. This methodology may also be applied to any other disease that results in these sequelae in the lungs.

Pulmonary high-resolution computed tomography examinations of 30 treated paracoccidioidomycosis patients were used in the study. The distribution of voxel attenuation coefficients was analyzed to determine the percentage of lung volume that consisted of emphysemic, fibrotic, and normal tissue. Algorithm outputs were compared with subjective evaluations by radiologists using a scale that is currently used for clinical diagnosis.

Affected regions in the patient images were determined by computational analysis and compared with estimates by radiologists, revealing mean ($\pm$ standard deviation) differences in the scores for fibrotic and emphysemic regions of $0.1\% \pm 1.2\%$ and $-0.2\% \pm 1.0\%$, respectively.

The computational results showed a strong correlation with the radiologist estimates, but the computation results were more reproducible, objective, and reliable.

(*Medicine* 93(25):e167)

Abbreviations: CAD = computer-aided diagnosis, COPD = chronic obstructive pulmonary disease, CT = computed tomography, HRCT = high-resolution computed tomography, HU = Hounsfield units, PCM = paracoccidioidomycosis.

INTRODUCTION

Currently, the evaluation of paracoccidioidomycosis (PCM) induced pulmonary alterations includes radiography, computed tomography (CT), and functional respiratory testing.[1,2] High-resolution CT (HRCT) provides additional information about the morphologic characteristics and distribution of pulmonary lesions, with advantages for the clinical diagnosis of lung diseases.[1,2] In the conventional evaluation of lung damage after disease treatment, a radiologist visually assesses the HRCT images, estimating the lung volume that is damaged by the disease. However, this approach is limited by intraobserver and interobserver variability.[3,4] Computer-aided diagnosis (CAD) systems may help produce objective measures of abnormal patterns in lung HRCT images, increasing confidence in the correlations between radiographic features and pulmonary diseases.[5]

PCM is a systemic mycosis that is caused by *Paracoccidioides brasiliensis*, a thermally dimorphic fungus that primarily produces disease in humans.[6,7] In South America, PCM is the most important endemic mycosis that is caused by *P brasiliensis*.[8,9] Brazil, Venezuela, and Colombia are endemic countries, and approximately 10% of the population in the subtropical regions of Brazil are affected.[8,9] The pathogen presumably grows in soil, constituting the infectious form that can cause disease in many organs and tissues.[10–13]

Pulmonary infection with PCM can cause a severe disease that uses the respiratory route as an entry portal,[14,15] followed by the formation of a primary complex, such as in tuberculosis.[16,17] In healthy individuals, the primary inoculation lesions may regress, with the persistence of viable fungi and formation of latent foci.[7,17] Reactivation of these foci can lead to chronic PCM, which typically has an insidious onset and slow evolution.[1,18] Although the disease remains localized in the lungs in some patients, most cases show a lymphohematogenous spread to other organs or systems.[1,14] PCM in the lungs can cause chronic obstructive pulmonary disease (COPD), the most common lung disease and a major cause of disability and death.[19] Although standard therapy is important in alleviating COPD symptoms, particularly dyspnea, many patients are left to cope with a chronic, irreversible, and disabling disease process.[19] Pulmonary rehabilitation is a well established means of enhancing standard therapy to control and alleviate symptoms, optimize functional capacity, and reduce the medical and economic burdens of disabling lung disease.[2,19]

The purpose of the present study was to employ a method for quantifying pulmonary fibrotic and emphysemic regions in the CAD context in treated PCM patients. A method was developed to classify and quantify normal, emphysemic, and fibrotic lung tissue. The results were compared with conventional visual estimates by a radiologist.

METHODS

Patient Selection

The present study was developed with ethical approval from the authors' institutions under protocol number 3883-2011. The research involved 30 patients with PCM, which was confirmed by the identification of typical *P brasiliensis* yeast forms at admission to the Infectious and Parasitological Diseases Service of the Medical School Hospital of Botucatu,

Editor: Angela Johnson.
Received: July 1, 2014; revised and accepted: September 10, 2014.
From the Departamento de Física e Biofísica, Instituto de Biociências de Botucatu, Univ Estadual Paulista (MA, MDO, JRAM); Departamento de Doenças Tropicais e Diagnóstico por Imagem, Faculdade de Medicina de Botucatu, Univ Estadual Paulista (DRP, SMR, RPM); and Centro Brasileiro de Pesquisas Físicas, CBPF/MCT (SBD).
Correspondence: Diana R. Pina, Univ Estadual Paulista Júlio de Mesquita Filho - UNESP, Botucatu, São Paulo, Brazil (e-mail: drpina@fmb.unesp.br).
The authors have no funding or conflicts of interest to disclose.

ISSN: 0025-7974
DOI: 10.1097/MD.0000000000000167

Universidade Estadual Paulista. PCM was detected by a positive finding of specific serum antibodies by a double agar gel immune diffusion test, together with radiological findings that suggested pulmonary involvement. Respiratory complaints and chest radiography showed interstitial and/or alveolar lesions, indicating a chronic character. Patients were eligible for the study if treatment with an anti-*P brasiliensis* compound was successful (reflected by a negative serum anti-*P brasiliensis* antibody result), and chest radiographs revealed fibrotic scars and different amounts of emphysema. Patients were ineligible for the study if they presented unsuccessful treatment or another systemic or pulmonary disease of any cause (eg, infectious, inflammatory, or neoplastic), with the exception of alcohol intake and cigarette smoking.

Data Acquisition

Images were obtained as retrospective HRCT scans on a helical CT scanner (SCT-7000TS, Shimadzu). Axial sections (1-mm thickness) were obtained at 10-mm intervals throughout the entire chest, with 20 to 30 slices acquired for each patient. No contrast agents were administered in the acquisition of the examinations.

An available set of 30 HRCT examinations of the patients' lungs was scanned. For each examination, the voxel distribution in Hounsfield units (HU) was obtained.

Radiologist Evaluation of the Images

Each HRCT examination in the patient sample was given to a radiologist who was skilled in thoracic CT and performed conventional visual estimates.[20] The same images were also passed through the semiautomatic computational quantification procedure. For comparison, the results were scored according to the amount of the injured pulmonary region that was detected by the scale that was used by the radiologist.

Fibrosis of the upper, middle, and lower lobes of the right lung and upper and lower lobes of the left lung were carefully and individually quantified by the radiologist and computational procedure using 6 scores from 0 to 5 (Table 1).[20] For the entire patient examination, emphysema tissue followed the scoring shown in Table 1, with 5 scores from 0 to 4.[21] This measurement was performed slice-wise, and the result was converted into a volume according to the slice separation size in the examinations.

Computed Algorithm

The algorithm followed a simple segmentation process described by Prionas et al[22] based on HU. Figure 1 shows a typical histogram that presents 3 well-separated characteristic peaks of the different tissues: around −800 HU for normal tissue, −950 HU for emphysemic tissue, and 70 HU for fibrotic tissue. Regions that were affected by pulmonary fibrosis and emphysema in the HRCT images were quantified by 4 computational steps.

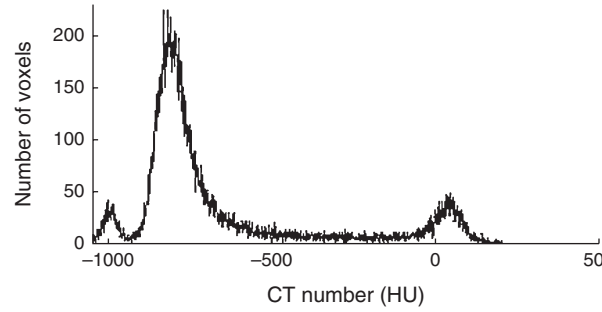

FIGURE 1. Histogram of a patient examination slice, exhibiting the characteristic peaks of normal, emphysemic, and fibrotic tissues. CT = computed tomography, HU = Hounsfield units.

First, the lung was manually segmented in each CT slice of the examination (Figure 2A and B). Although the literature has an extensive collection of articles, this step could not be completely automated because CAD procedures cannot automatically detect differences between fibrotic lung and soft tissues in the peripheral regions.[22–25]

In the second step, to emphasize the different tissues, the segmented lung was thresholded by analyzing the slice histogram, as shown in Figure 2C. The adopted pixel thresholds were the following: <-950 HU for emphysema, -600 to -950 HU for normal lung, and 0 to 150 HU for fibrosis.

In the third step, to quantify sequelae regions in the thresholded images, an opening operation (erosion followed by dilation) that used a disk with a 2 pixel radius was applied to remove small-sized areas that probably resulted from density fluctuations rather than lung abnormalities. This step resulted in an image with 4 gray levels: outside lung areas = 0, normal lung = 1, emphysema = −1, and fibrosis = 2.

Final quantification was performed by determining the regions of the differentially labeled pixels (ie, the classified lung volumes).

Creation of Software Phantoms

Algorithm procedures were kept as simple as possible. However, errors may be introduced during the computational process when evaluating tissues and determining their volumes since computational procedure applies morphologic operators and thresholding values. To estimate this error, comparing the results with a well known amount of lung tissue is necessary.

For this purpose, virtual phantoms, with established amounts of emphysemic and fibrotic tissues, were introduced on a normal lung tissue background. The involved regions were filled with a pseudorandom gray level that was sorted from the characteristic Gaussian distribution of each tissue in HU.[26] The generated image was subjected to the same procedural sequence as the one applied in the computational classification and evaluation of the patient tissue. The error was determined from the difference between the exact value implemented in the phantom and computational value.

TABLE 1. Score According to Percentage of Pulmonary Fibrotic Tissue (FS) (37–40) and Score According to Percentage of Pulmonary Emphysemic Tissue (41–44)

FS	Fibrosis	ES	Emphysema
0	Without fibrosis 0%	0	Without emphysema 0%
1	≤5% of the lobe	1	25% of the lung
2	6–24% of the lobe	2	50% of the lung
3	25–49% of the lobe	3	75% of the lung
4	50–75% of the lobe	4	>75% of the lung
5	>75% of the lobe		

EF = Emphysemic Score, FS = Fibrotic Score.

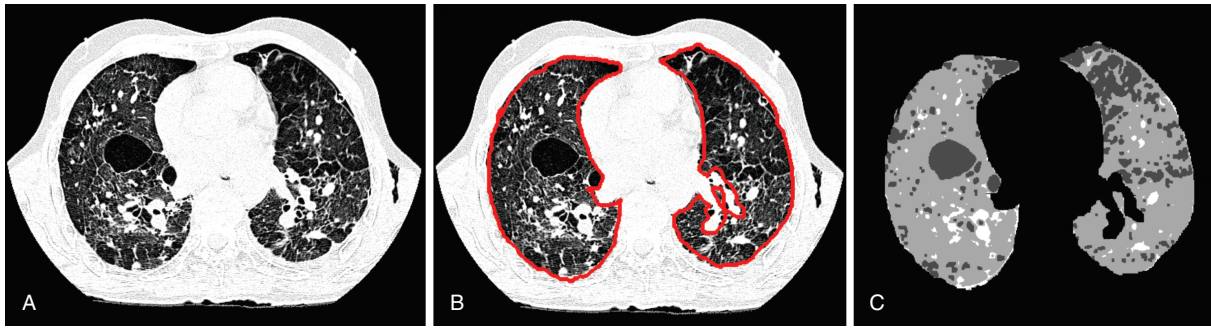

FIGURE 2. (A) Slice of lung exam used as input. (B) Segmented lung region after step 1. (C) Thresholded slice image, showing the result of step 2.

Three phantoms were generated with 20 slices each. The first phantom had 13% fibrotic tissue and 22% emphysemic tissue in completely separate regions. The second phantom had 17% fibrotic tissue and 33% emphysemic tissue in partially overlapping regions. The third phantom had 25% fibrotic tissue and 50% emphysemic tissue in completely overlapping regions. An example of the third phantom (25% fibrotic tissue and 50% emphysemic tissue) and the steps involved in its detection are depicted in Figure 3 in which a slice of the phantom with 12% simulated fibrotic tissue, 50% simulated emphysemic tissue, and 38% normal tissue was generated (Figure 3A). Manual segmentation of the lung region was performed by a radiologist and is presented in Figure 3B. The detection of the algorithm with 12.6% fibrotic tissue and 47.3% emphysemic tissue is shown in Figure 3C.

Radiologist and Algorithm Agreement

The results of the objective evaluation method that was developed to quantify the injured pulmonary region were compared with those from conventional subjective image assessment by a radiologist. The assessments from computed and visual evaluations were compared using Bland–Altman statistics[27] to assess agreement between the algorithm and reference standard, quantify the amount and direction of bias, and determine the upper and lower limits of agreement (bias $\pm$ 1.96 σ of the difference).

RESULTS

Computed Phantom Analysis

The computed phantom analysis yielded limits of agreement of $0.86\% \pm 0.38\%$, $2.55\% \pm 1.67\%$, and $2.50\% \pm 1.93\%$ for 13%, 17%, and 25% simulated fibrosis volumes and $2.1\% \pm 0.45\%$, $2.70\% \pm 1.83\%$, and $3.40\% \pm 1.38\%$ for 22%, 33%, and 50% simulated emphysema volumes.

Patient Analysis

Table 2 depicts the results for the 30 patients' examinations with visual and computed estimations of the lung volume, fibrosis volume, emphysema volume, and computed and visual assessments of the CT examinations. The fibrosis data were averaged among the 5 lung lobes, whereas emphysema had a unique score for the lung. The limits of agreement between computed and visual evaluations for the total lung evaluation (independent of lobes) were -0.2 ± 1.2 for fibrosis and 0.1 ± 1.0 for emphysema.

Figure 4 shows the Bland–Altman plots of the score difference between the radiologist and computed evaluations. Differences were not observed in the percentage of sequelae between lobes, although the evaluations of separate lobes for fibrosis were not important for the present study and are only presented to maintain the current form of the radiologist's evaluations.

DISCUSSION

Virtual phantom image analysis revealed that the computational evaluation procedure was significantly more precise than visual evaluation. The maximum mean error (3.40%) was small compared with the interval of the score scale that was used to quantify the tissues in the subjective radiologist evaluation.

An excellent level of agreement was achieved when the results of the computational method for the amounts of fibrosis and emphysema in patient lungs in a sample of 30 HRCT

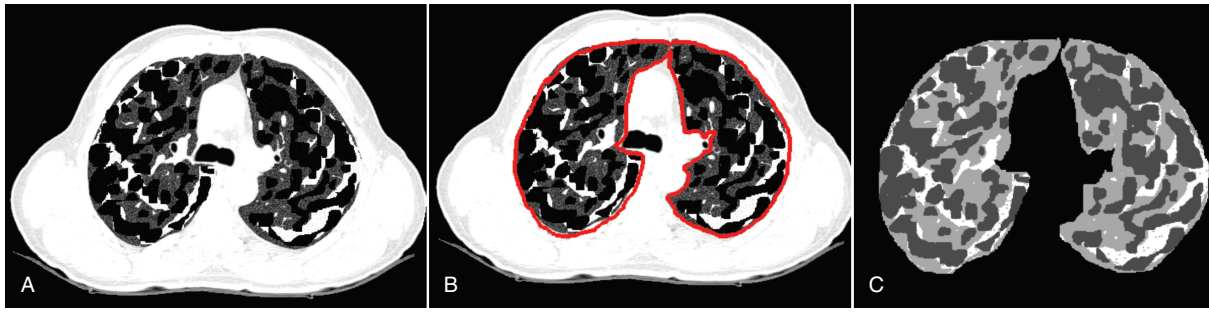

FIGURE 3. Example of the virtual phantom. (A) Slice of the phantom with 12% simulated fibrotic tissue, 50% simulated emphysemic tissue, and 38% simulated normal lung tissue. (B) Manual segmented lung region. (C) Segmented lung by the algorithm with 12.3% fibrotic tissue detected and 47% emphysemic tissue detected.

TABLE 2. Evaluation of the 30 Patients. Fibrosis Scores Were Averaged Along All of the Lobes With the Radiologist Evaluation, and Emphysema Scores Were Based on the Whole Lung and Not Divided by Lobes As With Fibrosis Scores

	Lung Volume (mm^3)				Score			
Patient No.	**Segmented**	**Fibrosis**	**Emphysema**	**Committed**	**RF**	**AF**	**RE**	**AE**
1	5.3×10^6	1.00×10^6	0.29×10^6	1.29×10^6	1.6	1.6	1	1
2	2.4×10^6	0.45×10^6	0.17×10^6	0.62×10^6	2.2	1.8	1	1
3	4.5×10^6	0.50×10^6	0.28×10^6	0.78×10^6	2.0	1.8	3	3
4	2.9×10^6	0.03×10^6	0.27×10^6	0.30×10^6	2.0	1.8	1	1
5	4.6×10^6	0.80×10^6	0.06×10^6	0.86×10^6	0.4	0.4	1	1
6	5.4×10^6	1.10×10^6	0.29×10^6	1.39×10^6	2.4	1.0	1	1
7	5.9×10^6	1.10×10^6	0.22×10^6	1.32×10^6	1.4	1.0	1	1
8	3.5×10^6	0.09×10^6	0.04×10^6	0.13×10^6	3.8	1.8	1	1
9	4.9×10^6	0.30×10^6	0.55×10^6	0.85×10^6	1.0	1.4	1	1
10	5.9×10^6	0.08×10^6	1.1×10^6	1.18×10^6	2.4	1.4	1	1
11	7.6×10^6	0.04×10^6	2.5×10^6	2.54×10^6	2.0	1.8	1	2
12	6.6×10^6	1.02×10^6	1.6×10^6	2.62×10^6	2.4	2.2	2	1
13	6.3×10^6	0.70×10^6	1.7×10^6	2.40×10^6	2.4	2.0	2	2
14	4.2×10^6	0.02×10^6	0.32×10^6	0.34×10^6	2.4	1.8	1	1
15	5.8×10^6	0.07×10^6	0.03×10^6	0.10×10^6	1.4	1.4	1	1
16	5.6×10^6	0.08×10^6	0.21×10^6	0.29×10^6	2.0	1.6	1	1
17	4.0×10^6	0.30×10^6	0.04×10^6	0.34×10^6	2.4	1.8	0	1
18	4.6×10^6	0.40×10^6	0.20×10^6	0.60×10^6	2.0	2.0	1	1
19	5.8×10^6	0.60×10^6	0.76×10^6	1.36×10^6	0.4	1.0	2	1
20	5.9×10^6	0.95×10^6	0.18×10^6	1.13×10^6	1.4	1.6	1	1
21	4.7×10^6	0.20×10^6	1.50×10^6	1.70×10^6	0.0	0.0	1	2
22	3.6×10^6	1.20×10^6	$0{,}14 \times 10^6$	1.34×10^6	2.6	3.0	1	1
23	5.8×10^6	0.29×10^6	0.64×10^6	0.93×10^6	1.0	1.0	1	1
24	5.3×10^6	0.12×10^6	0.58×10^6	0.70×10^6	0.2	1.2	1	1
25	5.3×10^6	0.02×10^6	2.4×10^6	2.42×10^6	3.2	3.0	2	2
26	6.1×10^6	0.08×10^6	0.04×10^6	0.12×10^6	1.8	1.4	0	0
27	5.8×10^6	0.02×10^6	0.00×10^6	0.02×10^6	2.6	1.8	0	0
28	4.0×10^6	0.02×10^6	0.21×10^6	0.23×10^6	0.8	0.8	0	1
29	5.7×10^6	0.30×10^6	1.40×10^6	1.70×10^6	0.0	0.0	1	1
30	6.2×10^6	1.30×10^6	0.09×10^6	1.39×10^6	0.0	0.0	1	1

AE = algorithm emphysema; AF = algorithm fibrosis; RE = radiologist emphysema; RF = radiologist fibrosis.

examinations were compared with the results of conventional radiologist evaluations that used the same scale. This agreement was mainly attributable to the simplicity of the technique applied because as increasingly more image processing techniques are applied to the image, increasing more parameters need to be adjusted. This procedure makes optimization very useful for one image and useless for another image with different structures and different aspects of the disease.

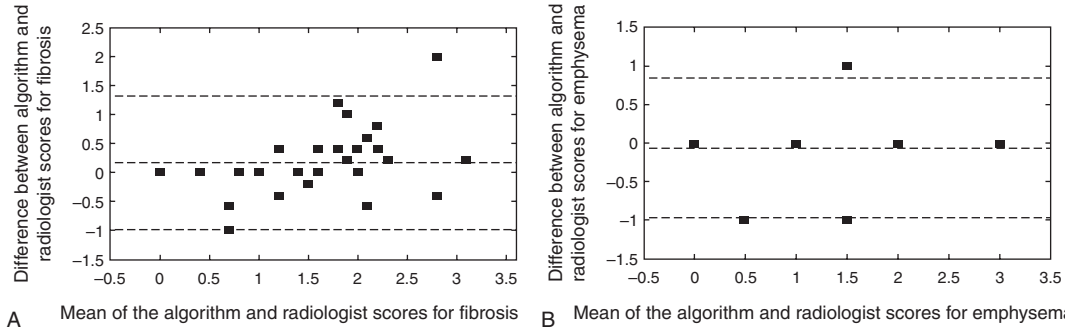

FIGURE 4. (A) Bland–Altman plots for scores of fibrosis and (B) emphysema. The difference refers to the reference standard minus the algorithm assessment. The difference between radiologist and algorithm scores was compared with the average score between the radiologist and computational results. Short dashed lines indicate the interval of 2 SDs, indicating an excellent level of statistical agreement between the results. Biases of (A) 0.1 ± 1.2 and (B) -0.2 ± 1.0, indicated by the dashed middle lines above the horizontal zero difference line, show that the reference standard is consistent with the results generated by the algorithms. SD = standard deviation.

Although no significant difference was found between the lobes, PCM fibrosis was slightly more prominent in the right middle and lower lobes. Radiologists confirmed this suspicion.

Our results suggest that this computational procedure offers a reliable, objective, and precise method that can be used to supplement visual grading, thereby providing a more advanced method for assessing sequelae in the lungs of treated PCM patients. When the subjective visual evaluation was used, the radiologist overestimated the areas that were affected by fibrosis or emphysema, corroborating the findings of Bankier et al.[28] Computers always follow determined steps when evaluating images, proving that the semiautomatic quantification method is more reproducible.[21] Notably, the algorithm can be used to aid in the clinical analysis of disease, permitting clinicians to identify differences among PCM sequelae. This method may also be applicable to COPD assessments, although more studies are needed. Prionas et al[22] reported that errors in volume quantification depend on the slice thickness. Our acquisition had a small slice thickness but a large increment between each slice, and encountering approximately 15% discrepancies between CT evaluations and real data is expected.

Some radiological findings in the lung due to pulmonary PCM are prominent in the pretreatment stage of the disease, such as cavitary nodules and ground-glass and tree-in-bud opacities. Septal thickening with architectural distortion and traction ectasias are prominent in the posttreatment stage.[29] Some of these patterns may cause confusion, depending on whether they are evaluated in the pretreatment or posttreatment stage. For example, ground-glass opacities may denote disease activity during the pretreatment stage or fibrosis when evaluated during the posttreatment stage.[8,29] To minimize variations, only patients who successfully received anti-*P brasiliensis* treatment were considered in this study.

The method that was used in the present clinical routine relies on subjective measurements with a low confidence level. These aspects can be significantly improved by using the semiautomatic objective method described in the present work.

PCM leads to fibrotic sequelae in the lung that increase the density at the lung boundary, affect soft tissue, and generate inaccuracies when automatically defining the lung boundary. Although the literature shows that some CAD procedures have been tested, all of them were based on the HU of the structure to be segmented.[22–25,30] Muscular tissue near the ribs and fibrosis present similar HU values, and the prior CAD methods failed to distinguish them. To overcome this limitation, lung edges were segmented manually.

CONCLUSION

The computational method presented in this study has great applicability to pulmonary involvement because evaluations are currently performed subjectively. Although PCM was the first disease to be quantified using this algorithm, these steps may be useful for any other pulmonary disease, such as idiopathic pulmonary fibrosis and COPD. Our results show that CAD schemes may greatly help radiologists follow patients with lung sequelae in general.

ACKNOWLEDGMENTS

The authors thank HC-FMB for support. The authors are also grateful to the Brazilian agencies CAPES, CNPQ, and FAPESP for their financial support.

REFERENCES

1. Lemle A, Wanke B, Mandel MB. Pulmonary localization of paracoccidioidomycosis: lung function studies before and after treatment. *Rev Inst Med Trop Sao Paulo.* 1983;25:73–78.
2. Ries AL, Bauldoff GS, Carlin BW, et al. Pulmonary rehabilitation: joint ACCP/AACVPR evidence-based clinical practice guidelines. *Chest.* 2007;131 (suppl 5):4S–42S.
3. Mannino DM, Homa DM, Akinbami LJ, et al. Chronic obstructive pulmonary disease surveillance: United States, 1971–2000. *Respir Care.* 2002;47:1184–1199.
4. Marchiori E, Valiante PM, Mano CM, et al. Paracoccidioidomycosis: high-resolution computed tomography-pathologic correlation. *Eur J Radiol.* 2011;77:80–84.
5. Bagci U, Bray M, Caban J, et al. Computer-assisted detection of infectious lung diseases: a review. *Comput Med Imaging Graph.* 2012;36:72–84.
6. Tani EM, Franco M. Pulmonary cytology in paracoccidioidomycosis. *Acta Cytol.* 1984;28:571–575.
7. Blotta MH, Mamoni RL, Oliveira SJ, et al. Endemic regions of paracoccidioidomycosis in Brazil: a clinical and epidemiologic study of 584 cases in the southeast region. *Am J Trop Med Hyg.* 1999;61:390–394.
8. Souza AS Jr, Gasparetto EL, Davaus T, et al. High-resolution CT findings of 77 patients with untreated pulmonary paracoccidioidomycosis. *Am J Roentgenol.* 2006;187:1248–1252.
9. Goldani LZ, Sugar AM. Paracoccidioidomycosis and AIDS: an overview. *Clini Infect Dis.* 1995;21:1275–1281.
10. Marques SA. Paracoccidioidomycosis: epidemiological, clinical, diagnostic and treatment up-dating. *An Bras Dermatol.* 2013;88:700–711.
11. Fiol FS, de Jesus Oliveira S, Barberato-Filho S, et al. Paracoccidioidomycosis: evaluation of treatment and patient profile. *Braz J Infect Dis.* 2013;17:720–721.
12. Lima TB, Domingues MA, Caramori CA, et al. Pancreatic paracoccidioidomycosis simulating malignant neoplasia: case report. *World J Gastroenterol.* 2013;19:5750–5753.
13. Duani H, Nunes VR, Assumpcao AB, et al. Bilateral paracoccidioidomycotic iliopsoas abscess associated with ileo-colonic lesion. *Rev Soc Bras Med Trop.* 2012;45:649–651.
14. Franco M, Peracoli MT, Soares A, et al. Host-parasite relationship in paracoccidioidomycosis. *Curr Top Med Mycol.* 1993;5:115–149.
15. Naranjo TW, Lopera DE, Diaz-Granados LR, et al. Histopathologic and immunologic effects of the itraconazole treatment in a murine model of chronic pulmonary paracoccidioidomycosis. *Microbes Infect.* 2010;12:1153–1162.
16. Severo KG, Oliveira Jda S, Carneiro M, et al. Latent tuberculosis in nursing professionals of a Brazilian hospital. *J Occup Med Toxicol.* 2011;6:15.
17. Bertoni TA, Perenha-Viana MC, Patussi EV, et al. Western blotting is an efficient tool for differential diagnosis of paracoccidioidomycosis and pulmonary tuberculosis. *Clin Vaccine Immunol.* 2012;19:1887–1888.
18. Lemle A, Wanke B, Miranda JL, et al. Pulmonary function in paracoccidioidomycosis (South American blastomycosis): an analysis of the obstructive defect. *Chest.* 1983;83:827–828.
19. Ries AL, Kaplan RM, Myers R, et al. Maintenance after pulmonary rehabilitation in chronic lung disease: a randomized trial. *Am J Respir Crit Care Med.* 2003;167:880–888.
20. Kazerooni EA, Martinez FJ, Flint A, et al. Thin-section CT obtained at 10-mm increments versus limited three-level thin-section CT for

idiopathic pulmonary fibrosis: correlation with pathologic scoring. *Am J Roentgenol.* 1997;169:977–983.

21. Goldin JG. Quantitative CT of the lung. *Radiol Clin North Am.* 2002;40:145–162.
22. Prionas ND, Ray S, Boone JM. Volume assessment accuracy in computed tomography: a phantom study. *J Appl Clin Med Phys.* 2010;11:3037.
23. Molinari F, Amato M, Stefanetti M, et al. Density-based MDCT quantification of lobar lung volumes: a study of inter- and intraobserver reproducibility. *Radiol Med.* 2010;115:516–525.
24. Sluimer I, Prokop M, van Ginneken B. Toward automated segmentation of the pathological lung in CT. *IEEE Trans Med Imaging.* 2005;24:1025–1038.
25. van Rikxoort EM, van Ginneken B. Automated segmentation of pulmonary structures in thoracic computed tomography scans: a review. *Phys Med Biol.* 2013;58:R187–R220.
26. Alvarez M, de Pina DR, Romeiro FG, et al. Wavelet-based algorithm to the evaluation of contrasted hepatocellular carcinoma in CT-images after transarterial chemoembolization. *Radiat Oncol.* 2014;9:166.
27. Bland JM, Altman DG. Statistical methods for assessing agreement between 2 methods of clinical measurement. *Lancet.* 1986;1:307–310.
28. Bankier AA, De Maertelaer V, Keyzer C, et al. Pulmonary emphysema: subjective visual grading versus objective quantification with macroscopic morphometry and thin-section CT densitometry. *Radiology.* 1999;211:851–858.
29. de Freitas RMC, Prado R, do Prado FLS, et al. Pulmonary paracoccidoidomycosis: radiology and clinical-epidemiological evaluation. *Rev Soc Bras Med Trop.* 2010;43:651–656.
30. Korfiatis P, Skiadopoulos S, Sakellaropoulos P, et al. Combining 2D wavelet edge highlighting and 3D thresholding for lung segmentation in thin-slice CT. *Br J Radiol.* 2007;80:996–1004.